PCCP

PERSPECTIVE

View Article Online
View Journal | View Issue

Features of the piezo-phototronic effect on optoelectronic devices based on wurtzite semiconductor nanowires

Cite this: *Phys. Chem. Chem. Phys.*, 2014, **16**, 2790

Qing Yang,†*[ab] Yuanpeng Wu,†[b] Ying Liu,†[a] Caofeng Pan[ac] and Zhong Lin Wang*[ac]

The piezo-phototronic effect, a three way coupling effect of piezoelectric, semiconductor and photonic properties in non-central symmetric semiconductor materials, utilizing the piezo-potential as a "gate" voltage to tune the charge transport/generation/recombination and modulate the performance of optoelectronic devices, has formed a new field and attracted lots of interest recently. The mechanism was verified in various optoelectronic devices such as light emitting diodes (LEDs), photodetectors and solar cells *etc.* The fast development and dramatic increasing interest in the piezo-phototronic field not only demonstrate the way the piezo-phototronic effects work, but also indicate the strong need for further research in the physical mechanism and potential applications. Furthermore, it is important to distinguish the contribution of the piezo-phototronic effect from other factors induced by external strain such as piezoresistance, band shifting or contact area change, which also affect the carrier behaviour and device performance. In this perspective, we review our recent progress on piezo-phototronics and especially focus on pointing out the features of piezo-phototronic effect in four aspects: *I–V* characteristics; *c*-axis orientation; influence of illumination; and modulation of carrier behaviour. Finally we proposed several criteria for describing the contribution made by the piezo-phototronic effect to the performance of optoelectronic devices. This systematic analysis and comparison will not only help give an in-depth understanding of the piezo-phototronic effect, but also work as guide for the design of devices in related areas.

Received 4th September 2013,
Accepted 11th November 2013

DOI: 10.1039/c3cp53737d

www.rsc.org/pccp

Introduction

Semiconductor nanowires have attracted a great deal of interest for their excellent geometric uniformity, subwavelength transverse dimension, and unique piezoelectric, photonic and electronic properties. The two-way coupling of photonics and electronics is the basis of optoelectronic devices such as optically/electrically pumped lasers,[1,2] nanowire LEDs,[3] ultrasensitive photodetectors[4] and high-efficiency solar cells.[5] The two-way coupling between mechanical force and photonics[6] has also been realized on subwavelength waveguides.[7] Recently, piezotronic devices which are based on the two-way coupling of electronic and piezoelectric properties have been attracting growing interest with a lot of applications in strain/force/pressure triggered/controlled electronic devices, sensors and logic units.[8–12] The concept of piezotronics, which utilises the piezopotential to act as a "gate" voltage to tune/control the charge transport behaviour, was first proposed by Z. L. Wang in 2007[8] and proved in various devices such as nanogenerators, piezotronic diodes and piezotronic transistors *etc.*[9–12] Furthermore, the coupling of the photonic, mechanical and electrical properties of semiconductor nanowires provides the possibility to improve the performance of optoelectronic devices[13–16] and to fabricate new functional devices[17,18] as well as to integrate optomechanical devices with piezotronic devices. A new field of piezo-phototronics is being formed.[19] The effect originates from the polarization of ions in a strained crystal with a non-central symmetric structure. When stress is applied, the relative centres of the cations and anions in the crystal are separated, resulting in a dipole momentum. The add-up of the dipole forms a piezo-potential.[19] The piezo-potential acts as a "gate" voltage to tune the charge transport/generation/recombination and modulate the performance of optoelectronic devices, which is called the piezo-phototronic effect. Since the concept was firstly proposed by Z. L. Wang in 2010,[20] numerous efforts have been devoted to this field, and the mechanism was verified on various optoelectronic devices.[11–18,20–24]

[a] *School of Material Science and Engineering, Georgia Institute of Technology, Atlanta, Georgia, 30332-0245, USA. E-mail: qingyang@zju.edu.cn, zhong.wang@mse.gatech.edu*
[b] *State Key Laboratory of Modern Optical Instrumentation, Department of Optical Engineering, Zhejiang University, Hangzhou 310027, P. R. China*
[c] *Beijing Institute of Nanoenergy and Nanosystems, Chinese Academy of Sciences, China*
† These authors contributed equally to this work.

For example: the responsivity of a ZnO micro-nanowire photodetector has been enhanced by a factor of 5.3 by the piezo-phototronic effect;[13] the conversion efficiency of an n-type ZnO nanowire/p-type GaN substrate LED has been improved by a factor of 4.25;[14] the efficiency of an n-CdS–p-Cu_2S core–shell nanowire (NW) solar cell has been enhanced by a factor of 1.7;[22] and so has the performances of photoelectron chemical cell[23] and the photoluminescence properties of a ZnO semiconductor nanowire[24] *etc.* J. H. Hao *et al.* demonstrated that acoustic and photonic dual mode emission could be induced by the piezo-phototronic effect in a PMN crystal.[17] These achievements not only demonstrate the way piezo-phototronic effects work, but also give rise to further research on their physical mechanism and potential applications. Simultaneously, other factors induced by external strain such as piezoresistance, band shifting, or contact area change can also affect the carrier behaviour and the device performance.[25] It is important to distinguish the contribution of the piezo-phototronic effect from other factors through comparison and theory analysis.

In this paper, we review our recent progress on piezo-phototronics and especially focus on pointing out the features of the piezo-phototronic effect, which will give a better understanding of previous experiments, and work as a guide for future work in related areas. We firstly define the material system that is suitable for the investigation of piezo-phototronics. Then the *I–V* characteristics of the device under piezo-phototronic effect are given. Subsequently, the dependence of the effect on the direction of the *c*-axis is described. Furthermore, the influence of the intensity of the illumination on the performance of the device is also analysed. Finally, we point out how piezo-phototronics can modulate the recombination–generation process of carriers. In the conclusion, we will summarize the features of the piezo-phototronic effect and propose several criteria for describing the contribution made by the piezo-phototronics effect to the performance of optoelectronic devices.

Material

In regard to piezoelectricity, readers may first think about lead zirconate titanate (PZT). PZT has found huge applications in electromechanical sensors, actuators and energy generators.[26] However, PZT is an electric insulator and thus less useful for building electronic devices. The second type of desirable material may be Si or Ge. They are extremely widely used in electronic devices, but could hardly provide a piezo-potential due to their symmetric structure. Through reading previous reports and deep investigation, we found that wurtzite structures such as ZnO, GaN, InN and AlN are suitable candidates for piezo-phototronics. Table 1 lists some useful parameters of materials that are worth investigating in piezo-phototronics. In the future, after careful design, doped PZT materials and quantum-well Si and Ge may become potential candidates for piezo-phototronics. Compared with crystal and film materials, one-dimensional nanomaterials, such as nanowires and nanobelts, are ideal for piezotronics and piezo-phototronics, as their elasticity range is much wider than the bulk material. Currently, the most popular material structure is ZnO nanowires (NWs) for three main reasons. First, ZnO NWs can be easily grown in large quantities using a vapour–solid-process or chemical approach at low temperature. Secondly, they are biologically compatible and environmentally friendly. Moreover, they can be grown on various substrates. In this review paper, we mainly summarise the piezo-phototronic effect on several important optoelectronic devices based on wurtzite structure semiconductor nanowires.

Table 1 Material parameters employed for some II–VI and III–V semiconductors in wurtzite phases. The lattice constants were calculated from the data in ref. 28 and 29; the elastic stiffness constants were obtained from ref. 30–33; the piezoelectric constants were obtained from ref. 32–37

	Lattice constant/Å	Permittivity constant	e_{31}, e_{33}, e_{15}/ C m^{-2}	C_{11}, C_{12}, C_{13}, C_{33}, C_{44}, C_{66}/10^{10} N m^{-2}
ZnO	*a*: 3.25 *c*: 5.21	n_o: 1.998 n_e: 2.015	e_{31}: −0.51 e_{33}: 1.22 e_{15}: −0.45	C_{11}: 2.31 C_{12}: 1.11 C_{13}: 1.04 C_{33}: 1.83 C_{44}: 0.72 C_{66}: 0.60
CdS	*a*: 4.135 *c*: 6.749	n_o: 2.342 n_e: 2.352	e_{31}: −0.244 e_{33}: 0.440 e_{15}: −0.210	C_{11}: 9.07 C_{33}: 9.38 C_{12}: 5.81 C_{13}: 5.10 C_{44}: 1.504 C_{66}: 1.630
CdSe	*a*: 4.30 *c*: 7.02	n_o: 2.552 n_e: 2.571	e_{31}: −0.160 e_{33}: 0.347 e_{15}: −0.138	C_{11}: 7.41 C_{33}: 8.36 C_{12}: 4.52 C_{13}: 3.93 C_{44}: 1.317 C_{66}: 1.445
GaN	*a*: 3.189 *c*: 5.185	n_o: 2.38 n_e: 2.31	e_{31}: −0.49 e_{33}: 0.73 e_{15}: −0.33	C_{11}: 4.077 C_{12}: 1.380 C_{13}: 0.752 C_{33}: 4.704 C_{44}: 1.023 C_{66}: 1.349
InAs	*a*: 4.284 *c*: 8.567	*n*: 3.808	e_{31}: −0.045 e_{33}: −0.028 e_{15}: 0.040	C_{11}: 1.103 C_{12}: 0.428 C_{13}: 0.321 C_{33}: 1.209 C_{44}: 0.273 C_{66}: 0.338
InP	*a*: 4.151 *c*: 8.301	*n*: 3.569	e_{31}: 0.103 e_{33}: 0.086 e_{15}: 0.071	C_{11}: 1.311 C_{12}: 0.513 C_{13}: 0.386 C_{33}: 1.438 C_{44}: 0.321 C_{66}: 0.399
AlN	*a* = 3.111 *c* = 4.978	n_o: 2.162 n_e: 2.209	e_{31}: −0.60 e_{33}: 1.46	C_{11}: 3.943 C_{12}: 1.465 C_{13}: 0.696 C_{33}: 4.704 C_{44}: 0.892 C_{66}: 1.239
InN	*a* = 3.544 *c* = 5.718	*n*: 2.9–3.05	e_{31}: −0.57 e_{33}: 0.97	C_{11}: 2.32 C_{12}: 1.15 C_{13}: 0.96 C_{33}: 2.39 C_{44}: 0.52 C_{66}: 0.59

I–V characteristics

The *I–V* characteristics of the piezo-phototronic devices are significant in that they can not only demonstrate the stability of the as-fabricated device but also can tell if the piezo-phototronic effect really occurs and how it works. In 2010, for the first time, we found an asymmetric change in the *I–V* curve of a single ZnO micro/nanowire metal–semiconductor–metal (MSM) photodetector when strain was applied,[13] which was proved to be one of the most important criteria[11,15] to distinguish the contribution of piezo-phototronics from other non-polarity factors[27] in further investigation.

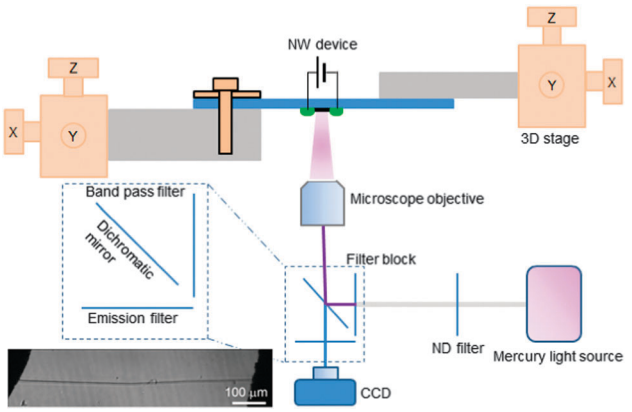

Fig. 1 Schematic diagram of the measurement system to characterize the performance of the piezopotential tuned photodetector. Reproduced with permission.[13] Copyright 2010, American Chemical Society.

The photodetector has an MSM structure with a ZnO wire bonded laterally to a polystyrene (PS) substrate. The electrodes are fabricated by fixing copper wires using silver pastes, then two back-to-back Schottky contacts form at the two ends of the wire (Fig. 1). We focused on the one with symmetric Schottky contacts at the two ends to ensure low noise and the ultra-sensitivity of the device (Fig. 2a). Then compressive/tensile strain is introduced by bending the substrate up and down, considering that the thickness of substrate is much larger than the diameter of the NW. The amplitude of the strain was calculated by measuring the maximum deflection of the free end of the substrate.

From Fig. 2b, we can see that the symmetry of the *I–V* curve in the dark does not show any obvious change under different compressive and tensile strain, which means the piezopotential has a small influence on the dark current. When the device is subjected to weak light UV illumination (less than 1 mW cm^{-2}), the asymmetric change of the *I–V* characteristics can be clearly seen with a variety of compressive and tensile strains. The absolute current at a negative bias increases step-by-step with the strain changing from 0.36% tension to −0.36% compression, while the current at a positive bias decreases (Fig. 2c and d). With the strain fixed at −0.36% compression strain, we can achieve the maximum enhancement of the responsivity of the photodetector of 530% under the illumination of 0.75 μW cm^{-2}. Utilizing the piezo-phototronic effect, the enhancement of a low dark current ultrasensitive UV photodetector has been realized.

The similar phenomenon of how piezo-potential modulates the *I–V* curve of a semiconductor device is also observed in electric pumped light emitting diodes (LEDs). The UV LED is mainly fabricated based on a ZnO NW–p-polymer inorganic–organic core–shell hybridized p–n junction.[15] The core–shell structure is coated with film electrodes separated by a well-controlled gap. The hybridized structure is across the two electrodes with ZnO NW on the cathode side and the core–shell structure on the anode side. The shell should terminate at the gap to avoid a short circuit (Fig. 3a). Fig. 3b shows the *I–V* characteristics of the as-fabricated device under no strain (the inset is the emission light captured by a CCD camera).

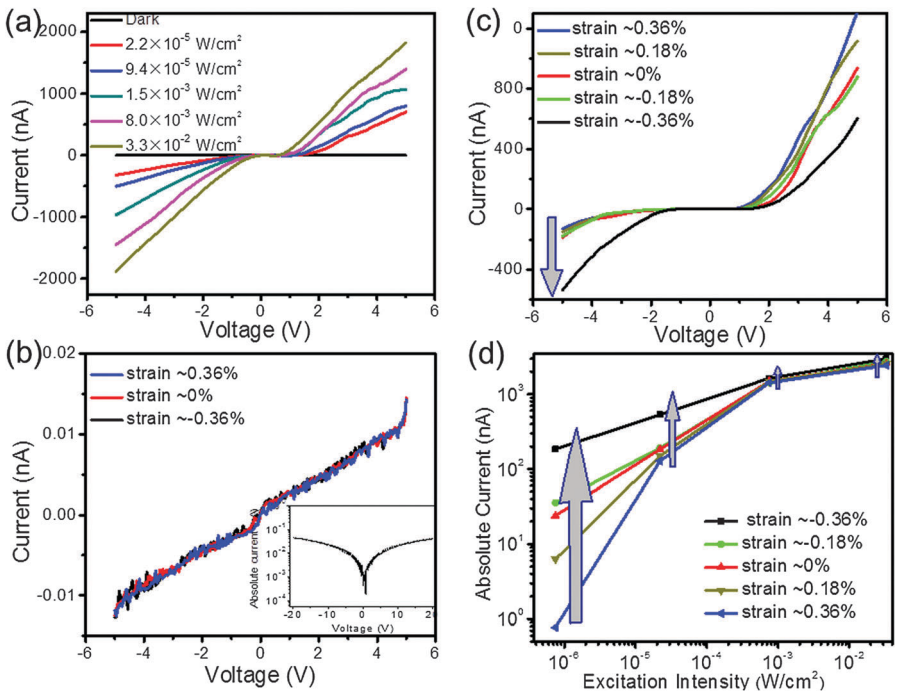

Fig. 2 (a) *I–V* characteristics of a single ZnO wire photodetector as a function of light intensity. (b) Typical dark *I–V* characteristics of a ZnO wire device under different strains. (c) *I–V* curves of the device under different strains with an excitation light intensity of 2.2×10^{-5} W cm^{-2}; the power illuminated on the nanowire was 120 pW, responsivity was increased by 190% under −0.36% compressive strain. (d) Absolute photocurrent relative to excitation intensity under different strain. Reproduced with permission.[13] Copyright 2010, American Chemical Society.

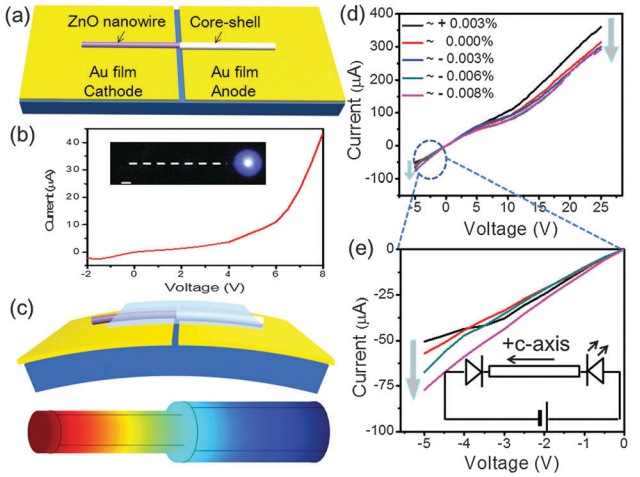

Fig. 3 (a) Schematic diagram of the device structure. (b) *I–V* curve of the LED, the inset is a CCD image of the LED at 25 V biasing voltage, and the dashed line represents the physical location of the ZnO NW–p-polymer core–shell structure, scale bar 10 μm. (c) Simulated piezo-potential distributions in the ZnO NW under tensile strain. (d) *I–V* characteristics of the device at forward bias with the variation of applied strain. (e) An enlarged picture of the *I–V* curve circled by a dashed line. Insets are the configuration of the device and direction of forward bias. Reproduced with permission.[15] Copyright 2013, American Chemical Society.

From the experimental data we found that the EQE (external quantum efficiency) and power conversation efficiency of the as-fabricated structure is about 1.6% and 0.5%. Subsequently, the characteristics of the *I–V* curve and emission light with various strains were further investigated. Fig. 3c shows the simulated piezo-potential distribution under tensile strain by using the finite element method. From Fig. 3d and e, we can see that with the strain changing from tensile to compressive, the current decreases under forward bias and increases at reverse bias. This asymmetric change of the *I–V* curve suggests that this phenomenon is mainly due to the piezo-phototronic effect, rather than the piezoresistance effect, band shifting, or the change of contact area, which would modulate symmetrically the current at both polarities of the biased voltage. In the experiments, we found, surprisingly, that although the forward-biased current decreases with increasing compressive strain, the intensity of emission of UV light increases exponentially with the strain, and the light is strong enough to be observed directly by the eye. The calculated enhancement of light intensity was 190% and the current deceased to 80% of the original value at −0.008% compressive strain, corresponding to an improved efficiency of 230%.

The experimental phenomena of the asymmetric *I–V* change that piezo-phototronic effects bring to semiconductor devices ask for a theoretical explanation. The core of our devices is usually a p–n or Schottky junction, which is subjected to an applied strain or illumination. Therefore, to investigate systematically the *I–V* characteristics of the device, the theory must treat semiconductor carrier transportation, piezoelectric effects and photoexcitation simultaneously. Take the theory for the Schottky contacts as an example. We begin our theoretical framework of the three-way coupling of piezo-phototronics by using a depletion approximation to treat the Schottky contact and assume that the piezo-charges uniformly distribute in the depletion region. The Schottky contact current equation was rectified by introducing coupling terms which represent the influence of photoexcitation effects and piezo-charges. The excess electrons and holes generated by photoexcitation would result in a split of the original equivalent Fermi level of the semiconductor into two quasi-Fermi levels for electrons and holes, respectively.[38,39]

$$E_{F_n} = E_F + kT\ln\left(\frac{n_0+\Delta n}{n_0}\right) \quad (1)$$

$$E_{F_p} = E_F - kT\ln\left(\frac{p_0+\Delta p}{p_0}\right) \quad (2)$$

where Δn, Δp represents the excess electrons and holes.

The impact of piezo-charges on the performance of the device can be analysed through how the piezo-potential modulates the Schottky barrier height (SBH). The modification to the SBH by piezo-charges is:

$$\Delta\phi_{\text{piezo}} = -\frac{1}{2\varepsilon}\rho_{\text{piezo}}W_{\text{piezo}}{}^2 \quad (3)$$

where ρ_{piezo} is the density of the strain-induced piezo-charges and W_{piezo} is the width of the distributed piezo-charges in the Schottky contact region.

For a single Schottky contact, the change of the height of the Schottky barrier due to photoexcitation effects and piezo-charges can be expressed as:

$$\Delta\phi_n = -\frac{1}{2\varepsilon}\rho_{\text{piezo}}W_{\text{piezo}}{}^2 - \frac{kT}{q}\ln\left(\frac{n_0+\Delta n}{n_0}\right) \quad (4)$$

And the corresponding electron current is:

$$J_n = J_{n_0}\left(\frac{n_0+\Delta n}{n_0}\right)\exp\left(\frac{q}{kT}\frac{1}{2\varepsilon}\rho_{\text{piezo}}W_{\text{piezo}}{}^2\right) \quad (5)$$

with J_{n_0} is the electron current under neither illumination nor external strain, and $J_{n_0} = A^*T^2\mathrm{e}^{-\frac{q}{kT}\phi_{n_0}}\left(\mathrm{e}^{\frac{q}{kT}V}-1\right)$, A^* is the Richardson constant, T is the temperature, q is the electron charge, ϕ_{n_0} is the original SBH and V is the applied voltage.

So the photoexcitation would reduce the SBH and increase the current at negative and positive bias symmetrically (Fig. 2a). Whether the piezo-charges enhance the current or reduce it depends on the direction of the *c*-axis and the type of applied strain, decided by the sign of ρ_{piezo}. When it comes to the case of double Schottky contacts, one of the Schottky junctions is forward-biased while the other one is reverse-biased. When the applied voltage is larger than the turning on voltage, the current behaviour is mainly dominated

by the reverse-biased contact. The reverse-biased Schottky current is:

$$J_n = J_{sv}\exp\left(-\frac{q}{E_0}\phi_{n_0}\right)\exp\left(\frac{q}{E_0}\frac{1}{2\varepsilon}\rho_{piezo}W_{piezo}^{2}\right) \times\left(\frac{n_0+\Delta n}{n_0}\right)^{\frac{kT}{E_0}}\exp\left(V_R\left(\frac{q}{kT}-\frac{q}{E_0}\right)\right) \quad (6)$$

where J_{sv} is the slowly varying term regarding changing voltage, E_0 is the tunnelling parameter and V_R is the voltage drop in the reverse contact. This equation indicates the asymmetric behaviour of the current under opposite biased voltage, which could be attributed to the opposite signs of ρ_{piezo} at the two ends of the wire.

Based on the proposed theory, we carried out numerical calculations for an Ag–CdS–Ag (MSM) structure. The parameters are reasonably set according to previous reports.[40] The calculated results show that for the photodetector with two opposite-biased Schottky junctions, the characteristics of the *I–V* curve clearly present asymmetric trends with increasing strain, just as the qualitative analytical results predicted (Fig. 4a). Meanwhile, the current has a symmetric change when there is just an increasing intensity of light illumination (Fig. 4b).

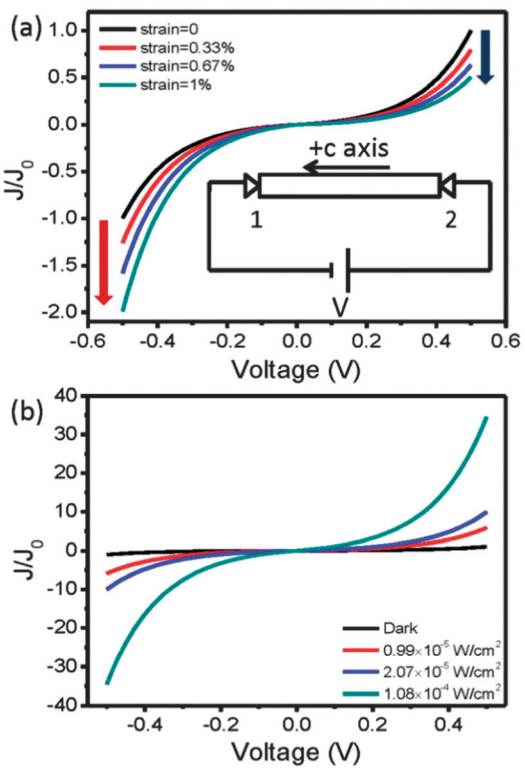

Fig. 4 Numerical simulation for a metal–CdS–metal photodetector with a Schottky contact on both ends based on our analytical solution. (a) Relative current density *vs.* voltage under different strains and the same illumination power. J_0 is set as the current of the device at zero strain and at reverse applied voltage of 0.5 V. Inset is the configuration of device and direction of forward bias. (b) Current–voltage diagram under different illumination powers. J_0 is set for the dark current at forward applied voltage of 0.5 V. Reproduced with permission.[41] Copyright 2012, American Chemical Society.

To further verify our theoretical framework, we have carried out some further experiments under the guidance of the calculated results. The data fit the theory well.

The *c*-axis orientation

In the experiments, we noticed that the compression strain or the tensile strain did not always improve the function of the device or make the performance worse. Take the photodetector we mentioned in Fig. 1 as an example. We found that some devices show an opposite change when applying the same strain. From Fig. 5a, we can see that the current under negative bias shows an opposite trend and decreases step-by-step with a variable strain changing from 0.26% tensile strain to −0.26% compressive strain under the same illumination of 0.75 μW cm^{-2}. Therefore, in this case it is the tensile strain rather than the compressive strain that enhance the responsivity of the photodetector. To make an easier understanding of this phenomenon, we firstly introduce the concept of the *c*-axis. In wurtzite structure nanowires, the *c*-axis is usually the polar direction of the wire. Therefore, when the wire is compressed/tensed by a mechanical force, a charge polarity forms at the two ends of the wire. Then, if the polar direction changes (the *c*-axis direction alters), a redistribution of the charge-generated piezopotential will result. Fig. 5b shows the piezopotential of the nanowires with different *c*-axes under the same force. In the case of LED, a similar phenomenon is also observed. Experimentally, when manipulating the nanowire for fabricating devices, we have approximately 50% of the *c*-axis of the nanowires along one direction and the other 50% along the opposite direction. Then, in the many devices we measured, about 50% of them had an enhancement effect, while the other 50% showed a reduction effect. The *c*-axis dependence can also be explained by our three-way coupling theory. The influence of the orientation of the *c*-axis is represented by the term ρ_{piezo} in eqn (6), whether the piezo-charges enhance the current or reduce depends on the direction of *c*-axis and the type of applied strain, that determines the sign of ρ_{piezo}. To clarify further this phenomenon, we carried out the numerical calculation for an Ag–CdS–Ag structure with one Ohmic contact and one Schottky contact. For simplicity, we tend to get the photocurrent *versus* different strain with the device forward-biased and under the same illumination. From Fig. 5c and d, we can see that the photocurrent can either increase or decrease with applied strain.

Last but not least, we present an intuitive understanding of the *c*-axis effects using the energy band diagrams. This time the solar cell is selected as an example. Solar cells are significant for the provision of the energy needed to sustain the development of human society. Moreover, solar energy is probably the most abundant clean and renewable resource. Nanowire photovoltaics can utilize the advantages of nanowires including a large surface to volume ratio, better charge collection, and the

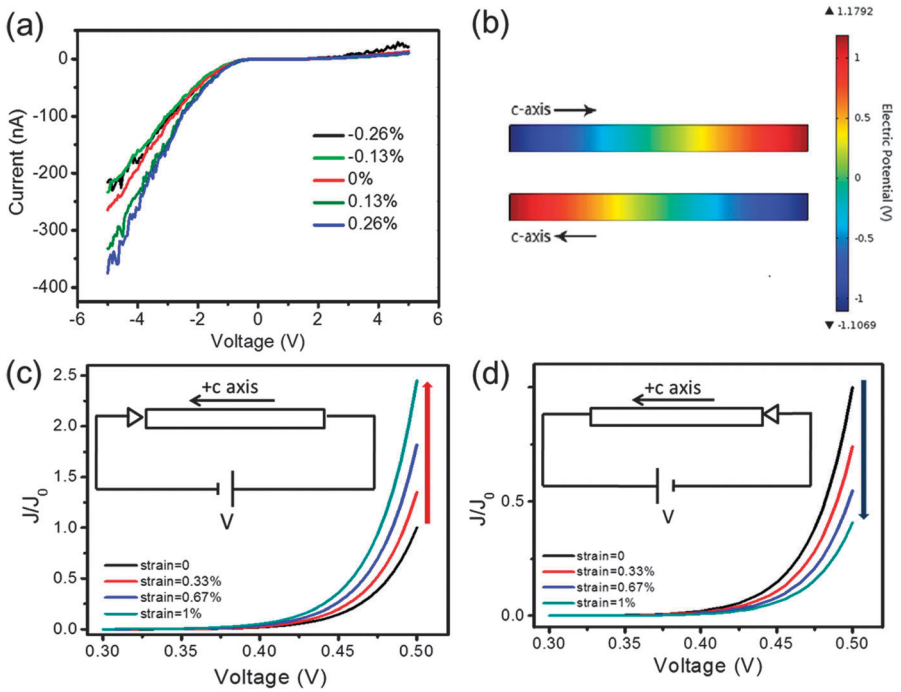

Fig. 5 (a) *I–V* curves of a ZnO single wire photodetector under different strain where the power illuminated on the nanowire is 6.4 pW and sensitivity is increased by 30% under 0.26% tensile strain. (b) The piezopotential of the nanowires with different *c*-axes under the same tensile strain. (c, d) Relative current density *versus* voltage under different strains and the same illumination power, for two devices with different orientations of the *c*-axis regarding the position of the Schottky contact. J_0 is set as the current of the device at zero strain and at an applied voltage of 0.5 V. Insets are the configuration of device and direction of forward bias. Reproduced with permission.[13,41] Copyright 2010/2012, American Chemical Society.

possibility of enhanced absorption through light trapping *etc.* The solar cells consist mainly of an n-CdS–p-Cu_2S core–shell NW and two silver pastes fixed at the both ends of the wire. To simulate accurately full-sun intensity (100 mW cm^{-2}), a solar simulator (300 W Model 91160, Newport) with an AM 1.5 spectrum distribution calibrated against a NREL reference cell was used. Fig. 6a–d present the performance, schematic structure and energy band structure of the coaxial photovoltaic (PV) device with structural configuration *I*.[22] We can found that the performance of this PV device was enhanced when it was subjected to a compressive strain up to −0.41%; and the I_{SC} and the V_{OC} under different strains were extracted and plotted in Fig. 6b. The I_{SC} increased from 0.25 to 0.33 nA, about 32% incensement; while the V_{OC} varying between 0.26 and 0.29 V, about 10% fluctuation. As dominated by the enhancement of the output current, the relative conversion efficiency of this PV device increased about 70% when a −0.41% compressive strain was applied (Fig. 6c). A theoretical model is proposed to explain the piezo-phototronic effect on the performance of the PV devices using energy band diagrams, as shown in Fig. 6d. The piezo-potential mainly drops along the axis of the nanowire under *c*-axis strain with the assumption of low-doping in CdS, for simplicity. For the first case, local positive piezo-charges form at the Cu_2S/CdS interface, which would increase Fermi level on the CdS side, leading to the decrement of the barrier height and the increment of the width of the depletion. Then, the separation of the electron–hole pairs would be accelerated and the recombination could be suppressed due to the enhanced internal field. On the contrary, for the second case, if the *c*-axis is changed and negative piezo-charges are generated at the interface, this just enhances the difficulty for electron–hole pair separation and decreases the output current and the conversion efficiency when applying the same strain.

Influence of the illumination and characteristics of emission

From the above we know that the *I–V* curve of the piezo-phototronic device presents just asymmetric behaviour with applied strain. In addition, it has been verified that piezo-phototronic effects can improve the sensitivity of the photo-detector and the efficiency of the solar cell. But in the experiments that were carried out, we also notice that the responsivity of the device is not be always the same when the illumination intensity is varied. Thus, how the performance of the device changes with a variety of illumination intensities is also investigated to give a deeper understanding of the piezo-phototronic effect. For the MSM structure photodetector, the transport dark current is dominated by the reverse-biased Schottky barrier and can be described by the thermionic-emission–diffusion theory as[39] (for $V \gg 3kT/q \approx 77$ mV):

$$I_{\mathrm{TED}}^{\mathrm{dark}} = SA^{*}T^{2}\exp\left[-\frac{1}{kT}\cdot\left(q\phi_{\mathrm{d}}^{\mathrm{dark}}\right)\right]\times\exp\left(\frac{1}{kT}\cdot\xi^{\frac{1}{4}}\right) \qquad (7)$$

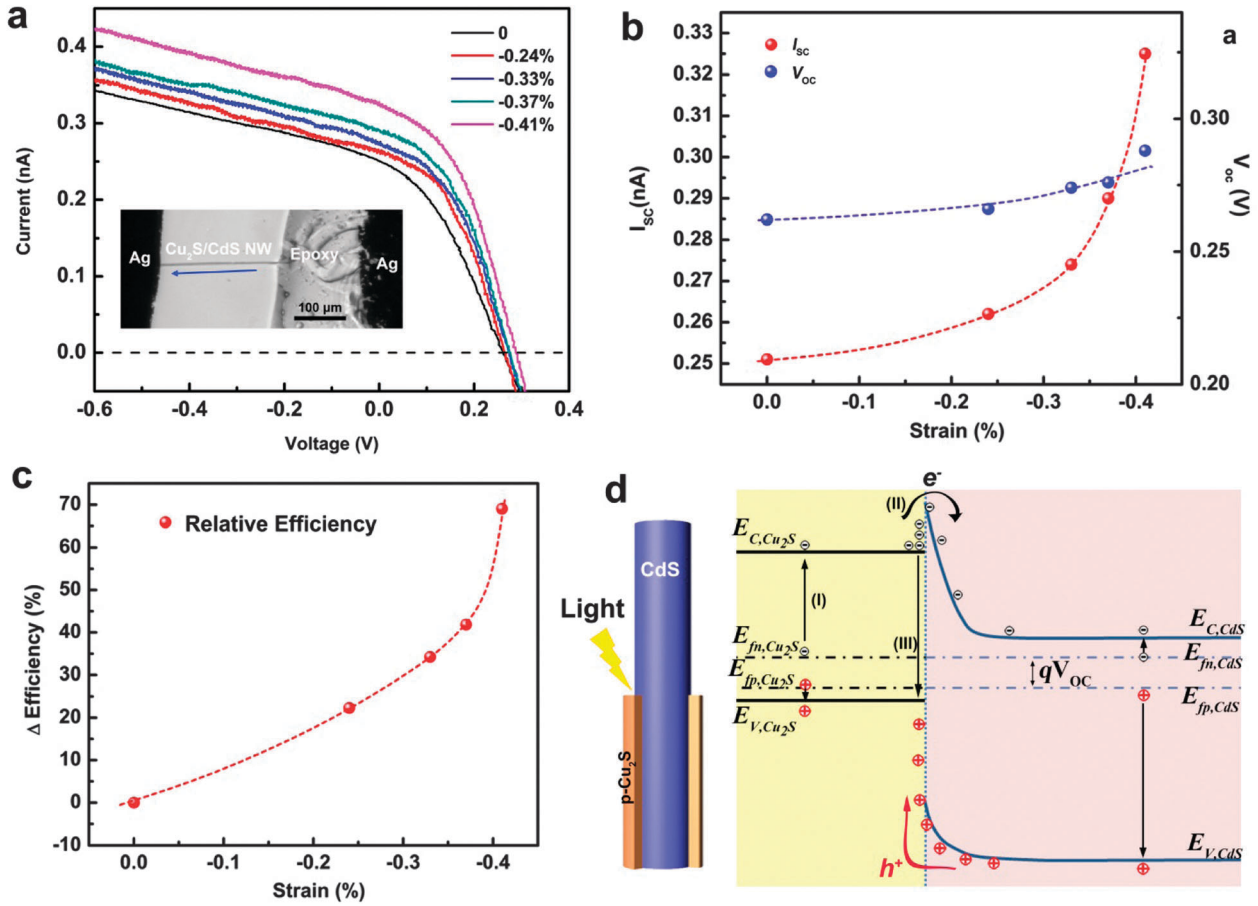

Fig. 6 The performance, schematic and energy band diagrams demonstrate the piezo-phototronic effect on a coaxial piezoelectric nanowire solar cells. (a) The *I*–*V* curve of the NW solar cell under different compressive strain, clearly indicating the current increase with increasing external compressive strain. The insert is an optical microscopy image of the Cu_2S/CdS coaxial NW solar cell. (b–c) Dependence of the open circuit voltage (b), the short circuit current (b) and relative efficiency change (c) on the strain. The data plotted in (b) and (c) are extracted from (a). (d) Schematics and the energy band diagram of a strain-free coaxial piezoelectric NW solar cell. Reproduced with permission.[22] Copyright 2012, American Chemical Society.

where $\xi = q^7 N_D (V + V_{bi} - kT/q)/8\pi^2\varepsilon_s{}^3$, $V_{bi} = \varphi_d^{dark} - (E_c - E_f)$, S is the area of the Schottky contact, A^* the effective Richardson constant, the temperature, k the Boltzmann constant, N_D the donor impurity density, V the applied voltage, V_{bi} the built-in potential and ε_s the permittivity.

The UV illumination could generate electrons and holes in the depletion region which would reduce the layer width. Besides, the shifted Fermi level could lead to a difference of energy barrier. The current transport with illumination can be described as:

$$I_{TED}^{ill} = SA^*T^2 \exp\left[-\frac{1}{kT}\left(q\phi_d^{dark} - (E_{FN} - E_F)\right)\right] \times \exp\left(\frac{1}{kT}\xi^{\frac{1}{4}}\right)$$
$$= SA^*T^2 \exp\left[\left(-\frac{1}{kT}\left(q\phi_d^{ill}\right)\right)\right] \times \exp\left(\frac{1}{kT}\xi^{\frac{1}{4}}\right) \quad (8)$$

where E_{FN} is the quasi-Fermi level under illumination.

Experimental results in Fig. 7a shows that the natural logarithmic scale current ln[I/(1 nA)] can be described by a power law of $V^{1/4}$ for the reverse-biased Schottky barrier. However, the red line, for the case of illumination, has a larger slope and higher extended zero points than the black line, without illumination. Combining with the eqn (7) and (8), this is mainly because the Fermi level E_F is raised to a quasi-Fermi level E_{FN} and the Schottky barrier height was decreased. The donor density N_D also increases due to holes generation in the depletion region. Fig. 7b shows the ln[I/(1 nA)] as a function of various strains with different excitation intensities. We found that the device under weaker illumination has a faster change of current under varying strain, as well as responsivity (Fig. 7c), corresponding to a faster change of the Schottky barrier height (Fig. 7d).

Besides clarifying the effects of excitation intensity on piezo-phototronic devices, the emission characteristics of LEDs are also investigated. Our micro/nanowire LED was fabricated by placing a ZnO wire across two sapphire substrates with same height, which were separated by a small distance. One of the substrates was coated with an Mg doped p-type GaN film fabricated by metal organic chemical vapour deposition (MOCVD) to form a p–n junction with an n-type ZnO wire side surface. The other substrate was coated with ITO to act as a cathode. The ZnO wire was covered by a transparent

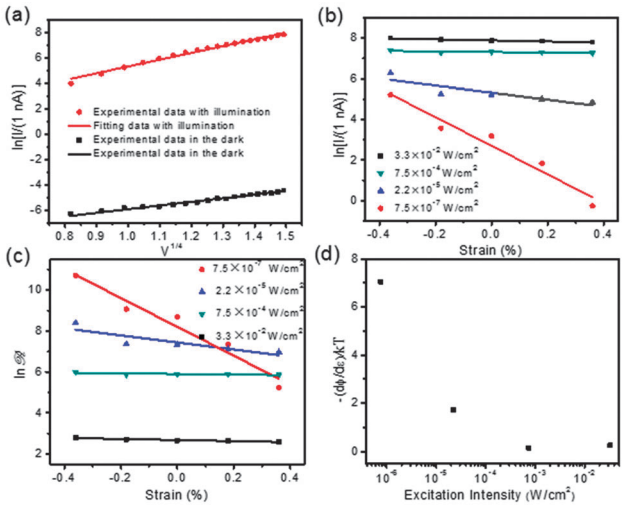

Fig. 7 (a) Plot of ln[*I*/(1 nA)] as a function of $V^{1/4}$, by using the data from Fig. 2b and c for the case of without strain. The red circles and line represent the experimental data and fitting curve with 3.3×10^2 W cm^{-2} light illumination. The black squares and line represent the experimental data and fitting curve in the dark condition. (b) Plot of ln[*I*/(1 nA)] as a function of strain under different excitation light intensity. (c) Responsivity (units A/W) as a function of strain under different excitation light intensity on a natural logarithmic scale. (d) The derived change of Schottky barrier height with strain as a function of excitation light intensity. Reproduced with permission.[13] Copyright 2010, American Chemical Society.

polystyrene (PS) tape to have a close contact with the GaN and ITO. We exploit an alumina rod connected to a piezo-nanopositioning stage to apply normally a mechanical force to the PS film. Therefore, such a uniformly normal force would result in compressive strain along the *a*-axis and tensile strain along the *c*-axis. Then, the polarization behaviour of the electroluminescence under applied strain is investigated. The spontaneous emission from the electric pumping LED distributes in a variety of polarizations, among which the $P_\perp$ mode dominates.[42] The propagating light along the wire would be reflected by the end-surface of the wire and the resonance phenomenon of the Fabry–Perot cavity occurs (Fig. 8d inset). When the strain along the wire is introduced, the optical length of the light is varied due to the change of the refractive index distribution in the wire. Therefore, the applying strain brings modulation in the interference pattern inside the wire and in the light emission. The large aspect ratio of the wire means the optical path for the $P_\parallel$ modes is much less affected compared with the $P_\perp$ modes. We define $\varnothing^{\parallel}_{out}$ and $\varnothing^{\perp}_{out}$ as representing light with a polarization direction parallel ($P_\parallel$ modes) and perpendicular ($P_\perp$ modes) to the wire, respectively. The ratio of $\varnothing^{\parallel}_{out}/\varnothing^{\perp}_{out}$ can be described by the Airy equation:[43]

$$\frac{\varnothing^{\parallel}_{out}}{\varnothing^{\perp}_{out}(\varepsilon)} \sim \left\{1 + \frac{4R}{(1-R)^2}\sin^2\left[\frac{\pi\left(2n_0L + n_0^3\beta E\varepsilon L_\varepsilon\right)}{\lambda}\right]\right\} \quad (9)$$

where R is the reflectivity of ZnO wire at the end-face, n_0 is its native refractive index without strain, L is the length of the wire, L_ε is the effective length of the wire under strain, β is the photoelastic coefficients, E is Young's modulus of ZnO, ε is the applied strain and λ is the light wavelength. Experimentally, we firstly obtained the relationship between the emission intensity and the rotation angle of the polarizer in reference to the orientation of the wire, as shown in Fig. 8a. Measurements of $\varnothing^{\parallel}_{out}/\varnothing^{\perp}_{out}$ are also carried out and the experimental data can be fitted by a function of a sine square. The results are consistent with our theory analysis (Fig. 8b and c). A simulation using eqn (9) in reference to the data presented in Fig. 8 derives the photoelastic coefficient $\beta \sim 3.2 \times 10^{-12}$ m^2 N^{-1} (at a wavelength of 395 nm) from the slope of the $\delta\varepsilon$ versus $1/L_\varepsilon$ curve, where $\delta\varepsilon$ is the strain period at which the $\varnothing^{\parallel}_{out}/\varnothing^{\perp}_{out}$ oscillates (see Fig. 8b). The β value is consistent with that reported for ZnO.[43–45] So, the applied strain on the LEDs can not only enhance the emission intensity but also modulate the polarization of the light propagating in the wire, which is called the piezo-photonic effect.

Modulation of carrier behaviour

Carrier behaviour, which mainly refers to the characteristics of the transportation, separation and recombination of the electrons and the holes in semiconductor devices, plays a key role in piezo-phototronics. Experiments aimed at modulating the behaviour of electrons and holes to achieve a significant improvement of the performance of the devices by tuning the height of the potential barrier were also carried out. In the as-fabricated ZnO–p-polymer core–shell NW LED, the unbalanced current between electrons and holes limits the recombination efficiency.[15] The straightest way to solve this problem is changing the structure of the device. In the experiments, we fabricated three devices by partially changing the material or the structure and making a comparison of their performances (Fig. 9).

The hybrid structure based on a nanoscale core–shell structure with Au electrodes has the highest EQE (external quantum efficiency); followed by the core–shell structure with ITO electrodes; the hybrid structure based on ZnO NW and ITO film electrodes has the lowest efficiency. The reason why Au electrodes function well can be explained by the energy band structure. The barrier height is 3.1 eV for holes and 1.3 eV for electrons when ITO is selected as the electrode. For Au these are 2.8 eV and 1.6 eV, respectively (Fig. 10a and b). Therefore, Au can balance the carriers current better by limiting the electrons and enhancing the injection of holes. The EQE of our ZnO–p-polymer core–shell structure is 1.6% and 0.3% for the structure using Au electrodes and ITO electrodes. The reason why a core–shell structure contributes a higher efficiency could be attributed to the more uniform contact formed at the ZnO/p-polymer interface.

Moreover, the piezo-phototronic effect is used to balance the current further. In the above, we have listed some occasions utilizing strain to improve the devices; essentially, the mechanism can be concluded to be the modulation effect that the strain has on the carrier behaviour. We still use the ZnO NW–p-polymer core–shell structure LED to clarify this concept.

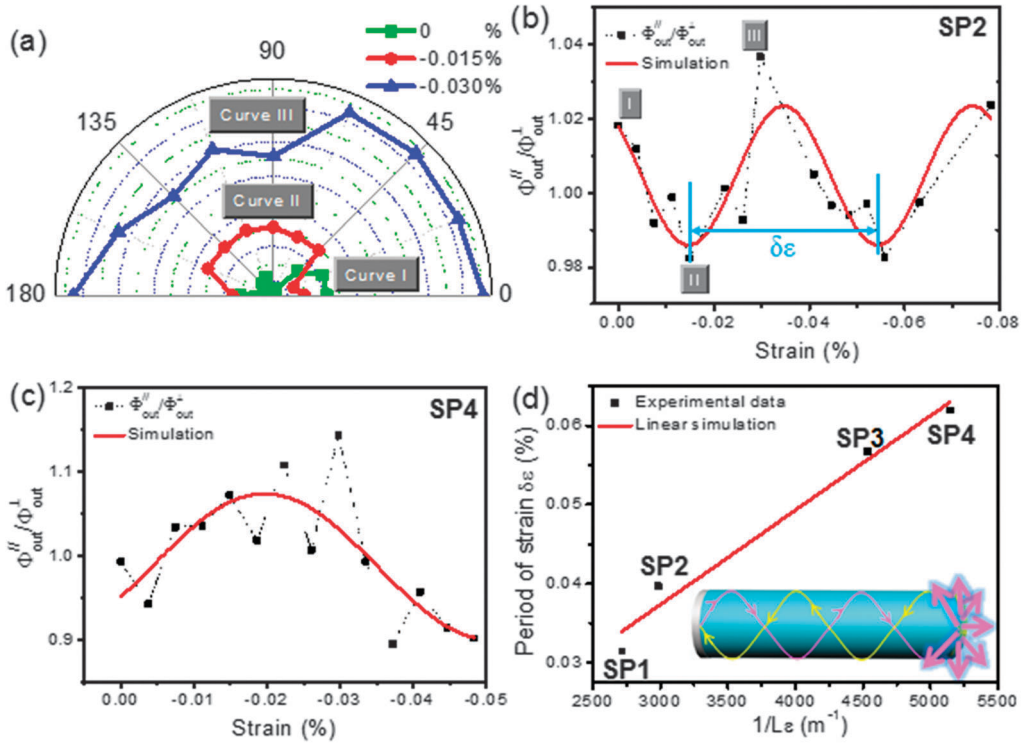

Fig. 8 Effects of strain on the polarization of the (n-ZnO wire)–(p-GaN film) emitted light, SP1, SP2, SP3 and SP4 stand for four independent samples. (a) Beam profile for the LED output under different strain as a function of the polarization angle. (b) The $\varnothing^{\parallel}_{out}/\varnothing^{\perp}_{out}$ ratio of the device used (a) under different strains, where the points corresponding to the curves I–III are labeled I–III. The period at which the intensity ratio varies is defined as $\delta\varepsilon$. (c) The $\varnothing^{\parallel}_{out}/\varnothing^{\perp}_{out}$ ratio of the device SP4 under different strain. (d) Plot of the measured strain varation period $\delta\varepsilon$ *vs.* the inverse of the effective length of the ZnO wire under strain. The inset shows a schematic standing wave within a Fabry–Perot cavity (ZnO wire) for the $P_{\perp}$ modes. Reproduced with permission.[14] Copyright 2011, American Chemical Society.

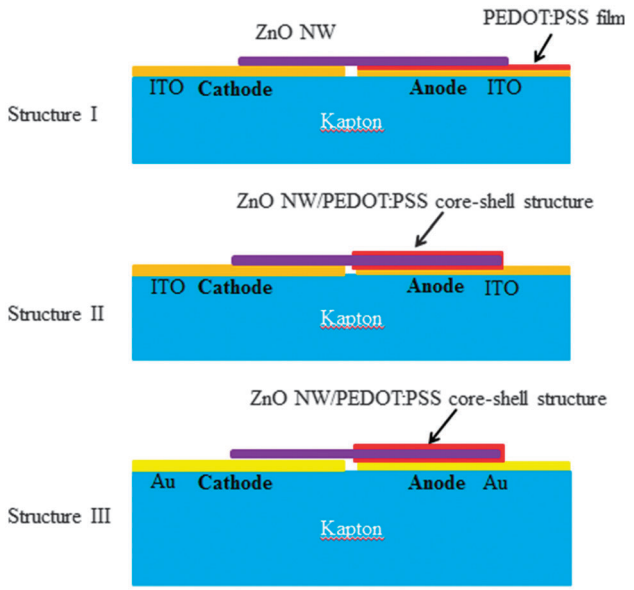

Fig. 9 Detailed side view of the three different kinds of device structures.

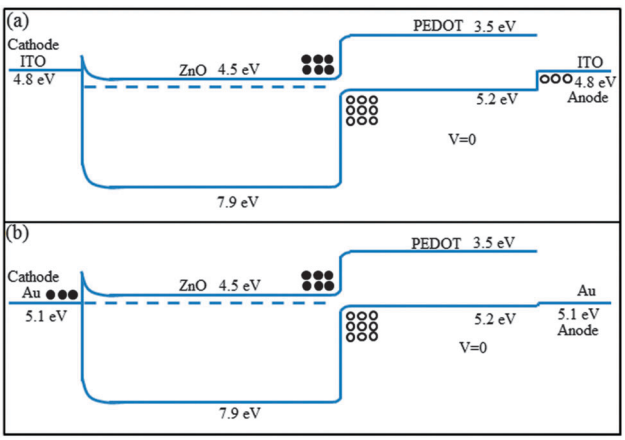

Fig. 10 Schematic energy band diagram of the LED without applied strain in thermal equilibrium using ITO (a) and Au (b) as electrodes, respectively. Reproduced with permission.[15] Copyright 2013, American Chemical Society.

We know that without strain, the total barrier height for holes is 2.8 eV, which is larger than the 1.6 eV of the electrons. So, there still exists a huge unbalanced density of electrons and holes, which is bad for the recombination efficiency. If the device is forward-biased, the Schottky barrier formed at the Au–ZnO contact surface was raised, which directly limits the transport of electrons and leads to the decrease of current. But the existence of piezoelectric charges can temporarily trap holes in the channel, which would contribute to the hole injection

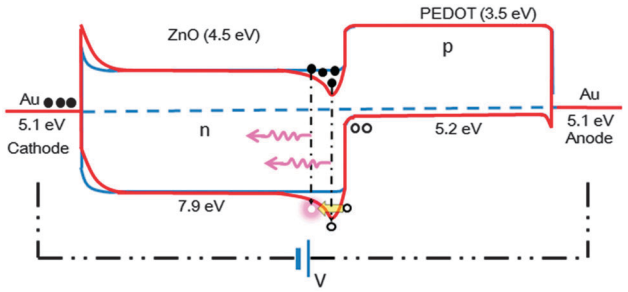

Fig. 11 Proposed mechanism of the enhanced light emission under strain for a ZnO NW–p-polymer core–shell UV LED under different strains. The red line represents the band diagram considering the piezo-phototronic effect, while the blue line represents the case without consideration of the piezo-phototronic effect. Reproduced with permission.[15] Copyright 2013, American Chemical Society.

from PEDOT:PSS to ZnO (Fig. 11). Therefore, the recombination efficiency near the junction is increased and the intensity of the emission light is enhanced.

Conclusion

In this review, we first briefly summarized the materials systems suitable for piezo-phototronic devices and then emphasized clarification of the features and application of piezo-phototronic effects from four aspects: the asymmetric characteristics of the *I–V* curve are investigated both from experiment and three-way coupling theory; although the piezo-phototronic effects can improve the performance of the semiconductor devices, we need to pay attention to the *c*-axis orientation in practical applications to avoid undesired failure; strong illumination can result in increased current, but will decrease the responsivity and piezo-phototronic effect for the photodetector, and this phenomenon means the piezo-phototronic effect is especially suitable for ultra sensitive weak-light photodetectors; how strain can modulate the polarization behaviour of the emission of LED has been shown; improved device structure can optimize carrier behaviour and thus emphasize the influence of the piezo-phototronic effect. In short, the enhancement to a device from piezo-phototronic effects is in nature a modulation of the transportation, separation and recombination of the carriers. Aside from the above the piezo-phototronic effect mechanism based on barrier height variation, a recently discovered mechanism based on the change of depletion region width is also important and requests further study.[16]

With the systematic three-way coupling theory and abundant experimental evidence, we have now an in-depth understanding of the piezo-phototronic effects, and we propose three criteria for charactering piezo-phototronics:

First of all, the existence of piezo-phototronic effects is based on the introduction of accumulated piezo-charges at the interface, such as the interface of the Schottky contact, the p–n junction and the junction where the lattice mismatch occurs. The photo-generated electrons and holes can change the quasi-Fermi level, which would lower the height of barrier and influence the piezo-phototronic effects significantly. Secondly, the effect is *c*-axis dependent; the effect may change from enhancement to reduction when changing the direction of the *c*-axis, and *vice versa*. Finally, if the devices have double reverse-orientated Schottky contacts, the presence of asymmetric behaviour in the *I–V* characteristics represents the existence of a piezo-phototronic effect.

Acknowledgements

This work is supported by National Natural Science Foundation of China (No. 61177062 and 51372220), National Key Basic Research Program of China (No. 2013CB328703), the Program for Zhejiang Leading Team of S&T Innovation and the Fundamental Research Funds for the Central Universities.

References

1 X. Duan, Y. Huang, R. Agarwal and C. M. Lieber, *Nature*, 2003, **421**, 241–245.
2 J. Li, C. Meng, Y. Liu and Q. Yang, *Adv. Mater.*, 2012, **25**, 833–837.
3 J. Bao, M. A. Zimmler, F. Capasso, X. Wang and Z. Ren, *Nano Lett.*, 2006, **6**, 1719–1722.
4 C. Soci, A. Zhang, B. Xiang, S. A. Dayeh, D. Aplin, J. Park, X. Bao, Y.-H. Lo and D. Wang, *Nano Lett.*, 2007, **7**, 1003–1009.
5 M. Law, L. E. Greene, J. C. Johnson, R. Saykally and P. Yang, *Nat. Mater.*, 2005, **4**, 455–459.
6 M. Eichenfield, J. Chan, R. M. Camacho, K. J. Vahala and O. Painter, *Nature*, 2009, **462**, 78–82.
7 M. Li, W. Pernice and H. Tang, *Nat. Nanotechnol.*, 2009, **4**, 377–382.
8 Z. L. Wang, *Adv. Mater.*, 2007, **19**, 889–892.
9 X. Wang, J. Song, J. Liu and Z. L. Wang, *Science*, 2007, **316**, 102–105.
10 G. Zhu, R. Yang, S. Wang and Z. L. Wang, *Nano Lett.*, 2010, **10**, 3151–3155.
11 W. Wu, X. Wen and Z. L. Wang, *Science*, 2013, **340**, 952–957.
12 J. Zhou, Y. Gu, P. Fei, W. Mai, Y. Gao, R. Yang, G. Bao and Z. L. Wang, *Nano Lett.*, 2008, **8**, 3035–3040.
13 Q. Yang, X. Guo, W. Wang, Y. Zhang, S. Xu, D. H. Lien and Z. L. Wang, *ACS Nano*, 2010, **4**, 6285–6291.
14 Q. Yang, W. Wang, S. Xu and Z. L. Wang, *Nano Lett.*, 2011, **11**, 4012–4017.
15 Q. Yang, Y. Liu, C. Pan, J. Chen, X. Wen and Z. L. Wang, *Nano Lett.*, 2013, **13**, 607–613.
16 J. Shi, P. Zhao and X. Wang, *Adv. Mater.*, 2013, **25**, 916–921.
17 Y. Zhang, G. Gao, H. L. Chan, J. Dai, Y. Wang and J. Hao, *Adv. Mater.*, 2012, **24**, 1729–1735.
18 C. Pan, L. Dong, G. Zhu, S. Niu, R. Yu, Q. Yang, Y. Liu and Z. L. Wang, *Nat. Photonics*, 2013, **7**, 752–758.
19 Z. L. Wang, *Adv. Mater.*, 2012, **24**, 4632–4646.
20 Y. Hu, Y. Chang, P. Fei, R. L. Snyder and Z. L. Wang, *ACS Nano*, 2010, **4**, 1234–1240.

21 Y. Hu, Y. Zhang, Y. Chang, R. L. Snyder and Z. L. Wang, *ACS Nano*, 2010, **4**, 4220–4224.
22 C. Pan, S. Niu, Y. Ding, L. Dong, R. Yu, Y. Liu, G. Zhu and Z. L. Wang, *Nano Lett.*, 2012, **12**, 3302–3307.
23 J. Shi, M. B. Starr, H. Xiang, Y. Hara, M. A. Anderson, J. H. Seo, Z. Ma and X. Wang, *Nano Lett.*, 2011, **11**, 5587–5593.
24 S. Xu, W. Guo, S. Du, M. M. Loy and N. Wang, *Nano Lett.*, 2012, **12**, 5802–5807.
25 A. Rowe, A. Donoso-Barrera, C. Renner and S. Arscott, *Phys. Rev. Lett.*, 2008, **100**, 145501.
26 S. Xu, B. J. Hansen and Z. L. Wang, *Nat. Commun.*, 2010, **1**, 93.
27 J. S. Milne, I. Favorskiy, A. C. H. Rowe, S. Arscott and C. Renner, *Phys. Rev. Lett.*, 2012, **108**, 256801.
28 I. Vurgaftman, J. R. Meyer and L. R. Ram-Mohan, *J. Appl. Phys.*, 2001, **89**, 5815.
29 K. Sarasamak, S. Limpijumnong and W. R. L. Lambrecht, *Phys. Rev. B: Condens. Matter Mater. Phys.*, 2010, **82**, 035201.
30 E. Deligoz, K. Colakoglu and Y. Ciftci, *Phys. B*, 2006, **373**, 124–130.
31 D. Berlincourt, H. Jaffe and L. Shiozawa, *Phys. Rev.*, 1963, **129**, 1009–1017.
32 J. Xin, Y. Zheng and E. Shi, *Appl. Phys. Lett.*, 2007, **91**, 112902.
33 S. Q. Wang and H. Q. Ye, *Phys. Status Solidi B*, 2003, **240**, 45–54.
34 W. Lee, M.-C. Jeong and J.-M. Myoung, *Nanotechnology*, 2004, **15**, 254–259.
35 F. Boxberg, N. Sondergaard and H. Q. Xu, *Nano Lett.*, 2010, **10**, 1108–1112.
36 S. de Gironcoli, S. Baroni and R. Resta, *Phys. Rev. Lett.*, 1989, **62**, 2853–2856.
37 F. Bernardini, V. Fiorentini and D. Vanderbilt, *Phys. Rev. B: Condens. Matter*, 1997, **56**, R10024.
38 E. H. Rhoderick and R. H. Williams, *Metal-Semiconductor Contact*, Clarendon, Oxford, 1988.
39 S. M. Sze and K. K. Ng, *Physics of semiconductor devices*, Wiley, 2006.
40 Z. Zhang, K. Yao, Y. Liu, C. Jin, X. Liang, Q. Chen and L. M. Peng, *Adv. Funct. Mater.*, 2007, **17**, 2478–2489.
41 Y. Liu, Q. Yang, Y. Zhang, Z. Yang and Z. L. Wang, *Adv. Mater.*, 2012, **24**, 1410–1417.
42 X. Guo, M. Qiu, J. Bao, B. J. Wiley, Q. Yang, X. Zhang, Y. Ma, H. Yu and L. Tong, *Nano Lett.*, 2009, **9**, 4515–4519.
43 M. Born and E. Wolf, *Principles of optics: electromagnetic theory of propagation, interference and diffraction of light*, CUP Archive, 1999.
44 J. Ebothe, W. Gruhn, A. Elhichou, I. Kityk, R. Dounia and M. Addou, *Opt. Laser Technol.*, 2004, **36**, 173–180.
45 K. Vedam and T. Davis, *Phys. Rev.*, 1969, **181**, 1196.

